Classification
Physics Abstracts
61.16D—68.55—73.40S

Structure of nickel thin films electrodeposited on n-GaAs single crystals

Luc Allemand, Michel Froment, Georges Maurin and Eliane Souteyrand

UPR15 du CNRS, Physique des Liquides et Electrochimie, Tour 22, 4 Place Jussieu, 75252 Paris Cedex 05, France

(Received 24 June 1992; accepted 23 October 1992)

Résumé. — Les courbes transitoires courant-temps résultant d'impulsions cathodiques, durant le dépôt électrolytique du nickel sur des monocristaux de GaAs, présentent une forme peu commune. On interprète les deux maxima du courant cathodique par un mécanisme de Stranski-Krastanov. Les observations en microscopie électronique par transmission et diffraction de surface des dépôts de nickel révèlent une croissance épitaxique en deux étapes, bidimensionnelle puis tridimensionnelle, donnant lieu à la formation d'arrangements spécifiques de macles.

Abstract. — Current *versus* time transients obtained by cathodic potential pulses, during nickel electrodeposition on n-GaAs single crystals, present an unusual, shape. The two maxima of the cathodic current are interpreted by a Stranski-Krastanov mechanism. TEM and RHEED observations of the nickel electrodeposits show the occurence of a two steps 2D/3D epitaxial growth with a multiple positioning of nuclei inducing the formation of specific twin arrangements.

Introduction.

Electrocrystallization of metals on semiconducting electrodes received recently a special interest for microfabrication processes applied to microelectronics. During the first step of the electrocrystallization process the charges transit towards the surface through the surface states located in the band gap. But as soon as a critical density $\left(10^{10}\ \mathrm{cm}^{-2}\right)$ of crystallites on the surface is reached the semiconducting electrode behaves like a Shottky contact and the charge pathway passes *via* the metallic islands. Therefore the semiconducting nature of the substrate comes into play only at the very beginning of the nucleation [1].

When the metal deposition kinetics is controlled by mass transport (silver, copper), the impoverishement of metallic ions inside the hemispherical diffusion layer surrounding the first born crystallites, drastically diminishes the probability of nucleation and create areas free of metal nuclei [2]. It results that the coalescence of the crystallites is impedded whatever the nature of the

substrate. On the contrary the deposition kinetics of metals like nickel is controlled by the charge transfer reaction rate. When nickel is deposited on a neutral substrate like glassy carbon the current-time transient obtained in response to the application of a potentiostatic pulse shows the existence of one maximum. This curve has been interpreted by the formation and the growth of three dimensionnal nuclei (3D) on the rising part of the current followed by the coalescence of the nuclei when the maximum of the current is reached [3] and finally, the current tends to a stationary value when the surface is completly covered by coalesced crystallites. SEM and TEM observations gave an experimental evidence of this interpretation.

A completely different situation is found when nickel is electrodeposited on (100) or (111) GaAs. Figure 1 shows that the current goes through two maxima. The second one, observed after approximatively 10 secondes, can be clearly compared to the maximum found in the same time range during nickel deposition on glassy carbon [3]. It corresponds to the nucleation, the growth and the coalescence of 3D nuclei. The first maximum is very sharp and corresponds to a quantity of electricity allowing the deposition of 2-4 nickel monolayers. The shape of the first part of the transient curve is in good agreement with the model of a bidimensional nucleation followed by a lateral growth which continues until the complete surface coverage [4]. By plotting the rising part of the first maximum in logarithmic coordinates, straight lines with a slope near 1 is found, corresponding to an instantaneous 2D nucleation. Then the overall process can be interpreted by a Stranski-Krastanov mechanism [5]. The aim of this paper is to determine, thanks to TEM and RHEED observations, the morphology of the deposits and the orientation relations between nickel and GaAs single crystals taking in account the peculiarities of the current-time curve.

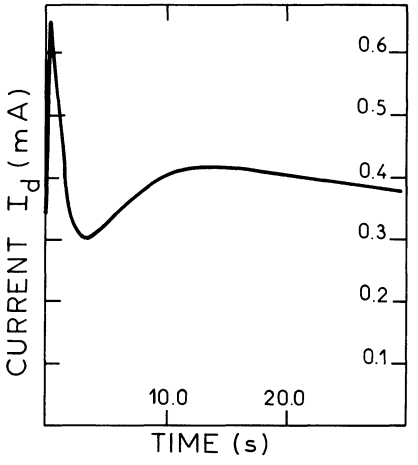

Fig. 1. — Current-time transient for nickel deposition on (100) n-GaAs; cathodic potential $V_d = -0.9$ V/SCE.

Experimental.

GaAs SUBSTRATES. — Semiconducting electrodes are made of single n-GaAs crystals (100) or (111) oriented with a doping level c.a. 10^{16} cm^{-3}. Compacts (111) planes are alternatively constituted of one single type of atoms (Ga or As). By convention, (111) represents the Ga plane and

$(\bar{1}\bar{1}\bar{1})$ is relative to the As plane. The Au-Ge back ohmic contact is prepared by vacuum evaporation and annealed at 400 °C under N_2. The active surface is mechanically polished with 1 μm diamond paste and chemically etched with the usual mixture (H_2O ; H_2O_2 ; H_2SO_4) (Vol 25; 2; 2) at room temperature. Just prior the deposition, working electrode is dipped into a 0.1% Br_2-MeOH solution, rinsed in desionized water and dried under argon.

NICKEL ELECTRODEPOSITION. — Nickel is deposited from a Watts' solution containing 300 g/l ($NiSO_4$, $7H_2O$), 35 g/l ($NiCl_2$, 6 H_2O) and 40 g/l H_3BO_3. The solution is thermostated at 50 °C. The cathodic potential is monitored, with respect to a saturated calomel electrode, by an electronic potentiostat. The cathodic potential step is generated by a wave form generator. Current *vs.* time transients are registered with a digital recorder.

STRUCTURAL INVESTIGATIONS. — Structural investigations have been managed in relation with the peculiarities of the cathodic current-time curve (Fig. 1). As the nickel deposit formed after the first maximum is very thin (2-4 monolayers), the preparation of extractive replicas is very difficult. Crystallographic relations between nickel and GaAs have been studied thanks to RHEED observations. For thicker deposits, corresponding to the second part of the transient curve, extractive replicas have been prepared: a thin and continuous carbon film is evaporated on the nickel deposit and stripped off the substrate thanks to the superficial dissolution of GaAs into a Br_2MeOH solution. In some cases a thinning of the nickel deposit on GaAs has been performed by ion milling. TEM observations were carried out with a 100 kV (JEOL 100 CX2) and a high resolution 200 kV (JEOL 2000FX) microscopes.

Results.

THIN NICKEL FILM ON A (100) GaAs FACE. — Thin Ni deposits which correspond to the first step of the Stransky-Krastanov process were observed by reflexion electron diffraction. Their thickness is so small that the diffraction pattern of the GaAs substrate is also visible. It can be easily recognized thanks to its diffuse streaks characteristic of a flat single crystal surface. In order to identify nickel orientation relatively to the GaAs crystal, RHEED diffraction patterns were recorded for several azimuthal directions, by rotating the sample in the microscope column. Nickel diffraction spots are more diffuse. Whatever the azimuth, a (220) Ni diffraction spot is always present on the symmetry axis of the diagramm. In other words, (110) planes of the nickel layer are parallel to the substrate surface. The following epitaxial relation can therefore written as:

$$(100)\ \text{Ni} \,//\, (100)\ \text{GaAs} \qquad (1)$$

For the pattern presented in figure 2a, the incident electron beam was parallel to the $[01\bar{1}]$ axis of the GaAs crystal face. The diagramm is a $(1\bar{1}2)$ section of the reciprocal lattice of nickel. The [111] Ni axis seems in coincidence with the $[0\bar{1}\bar{1}]$ GaAs axis. Figure 2c presents a schematic representation of the diffraction pattern. In these conditions, the second relation defining Ni (100)/GaAs epitaxy would be:

$$[111]\ \text{Ni} \,//\, [011]\ \text{GaAs} \qquad (2)$$

However, because of the lack of precision in the determination of the azimuthal angle of the incident beam, this relation can't be considered as totally established.

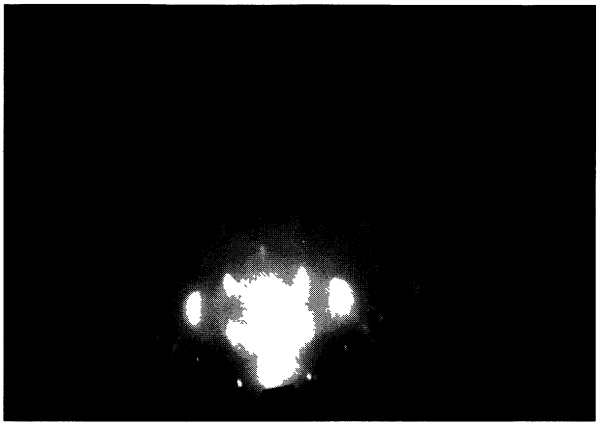

a)

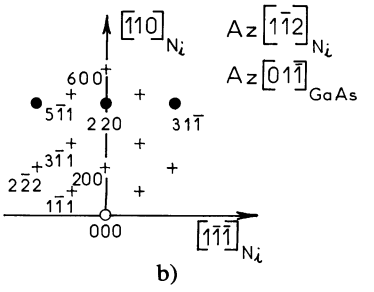

b)

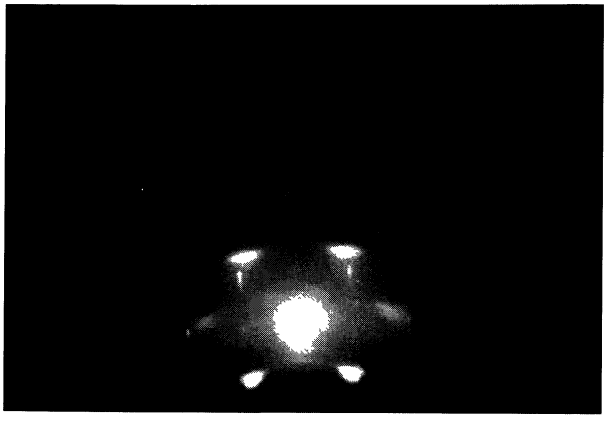

c)

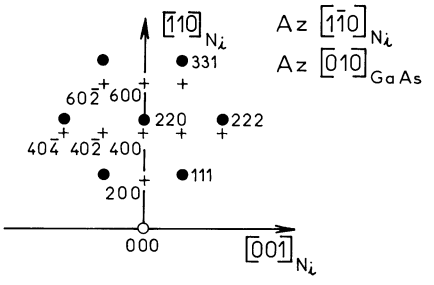

d)

Fig. 2. — RHEED diagrams obtained with a thin nickel film deposited on (100) n-GaAs. (a) Observation in the [01$\bar{1}$] GaAs azimuth. (b) Indexation of the diagram (a). (c) Observation in the [010] GaAs azimuth. (d) Indexation of the diagram (c). (+) GaAs diffraction spots, (•) Ni diffraction spots.

The diffraction pattern obtained with the same sample but with a incident beam parallel to the [010] GaAs axis is showed in figure 2c. Nickel diffraction spots belong to the [1$\bar{1}$0] section of the reciprocal lattice. The [001] Ni axis is parallel to the projection of the sample surface and seems to coincide with the [001] GaAs axis. This last relation appears as unlikely, knowing that the misfit between (300) GaAs and (200) nickel interreticular distances is as large as 5% whereas it is only 1.8% between (220) GaAs and (111) Ni interreticular distances. We can conclude that the first hypothesis described by equation (2) is the most satisfying.

A more detailed examination of figure 2a pattern allows to distinguish few Ni diffraction spots which do not belong to the epitaxial model corresponding to equations (1) and (2). In particular, two faint (100) spots symmetrically are located on both sides of the symmetry axis. We may assume that a small quantity of nickel would follow an other epitaxial relation which is characterized by a (100) Ni plane making a small angle (c.a. $\pm$ 15°) with the (100) GaAs face. In order to confirm the validity of the hypothesis of the presence of a tilt boundary between the two materials, it would

a)

b)

Fig. 3. — TEM observation of a nickel deposit on (100) n-GaAs; $V_d = -0.9$ V/SCE, $t_d = 30$ s. (a) Bright field image. (b) Dark field image. (c) Microdiffraction diagram corresponding to (a). (d) Indexation of diagram (c) : (o) GaAs diffraction spots; (•) Ni diffraction spots belonging to one (110) unit cell; (+) Ni diffraction spots belonging to the other positions of the (110) unit cells. (□) Ni diffraction spots corresponding to a (100) epitaxial pattern.

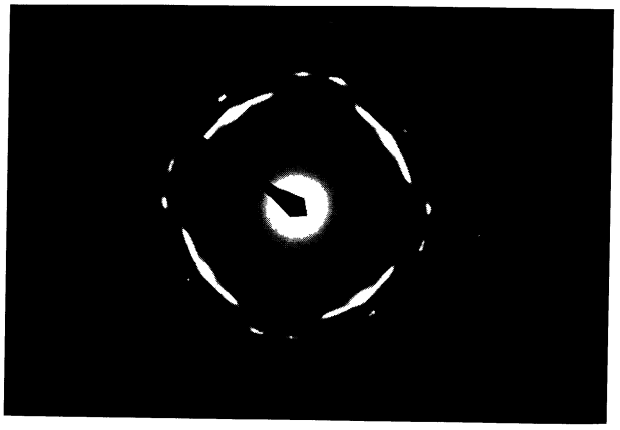

c)

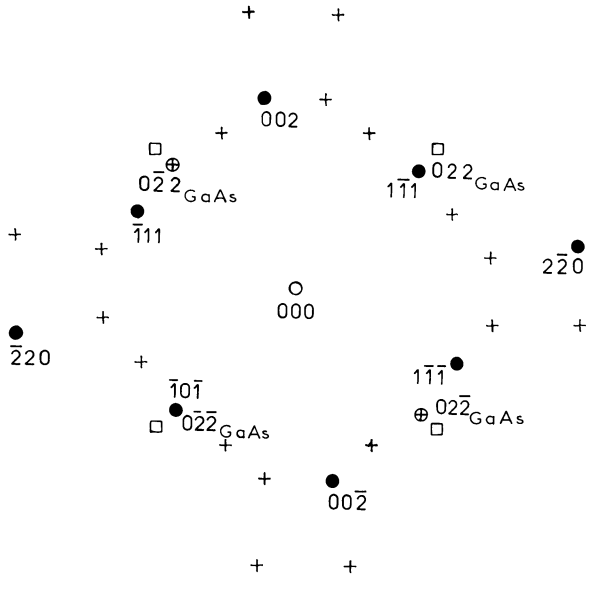

d)

Fig. 3. — continued.

THICK NICKEL LAYER ON A (100) GaAs FACE. — Nickel coatings electrodeposited during a time sufficiently long to be sure that the coalescence of 3D crystallites is completely achieved, were examined by bright and dark field TEM imaging. On the micrographs presented in figures 3a and 3b one can see that the nickel film is made of 20 to 30 nm in diameter microdomains, which often contain vertical twin lamellae. The associated transmission diffraction pattern is quite complex (Fig. 3c), it exhibits a general fourfold symmetry. Faint diffraction streaks due to twin lamellae facilitate the indexation of crystal directions. A detailed analysis of this pattern coupled with dark field imaging allowed us to reconstitute the model diagramm of figure 3d. In fact, it consists in the superposition of four (110) Ni diagramms, all of them are fulfilling the epitaxial relations (1) and (2). It is worth noting that the 3D nucleation of the second step of the Stransky-Krastanov

process conserves the epitaxial orientation of the first Ni underlayer. In few samples, where the GaAs substrate was not completely eliminated by ion milling the observation of moire patterns confirmed the validity of equation (2). The four equivalent positions A1, A2, B1 and B2 of nickel crystals relatively to the (100) GaAs face are schematically presented in figure 4. For the sake of clarity, Ni crystals were supposed to be limited by $[1\bar{1}2]$ and $[1\bar{1}0]$ atomic rows. For A1 and A2 positions the $[1\bar{1}2]$ atomic row coincides with the [011] GaAs axis, for B1 and B2 it coincides with the $[0\bar{1}1]$ axis. Crystals in positions A1 and A2 (or B1 and B2) are symmetric versus a vertical $(1\bar{1}\bar{1})$ plane. When during their growth they enter in contact, they form vertical $(1\bar{1}\bar{1})$ twin boundaries. Figure 5 shows a high resolution TEM micrograph where (111) atomic planes of two neighbourhing crystals in twin position are well visible and are symmetric with respect to the central twin boundary.

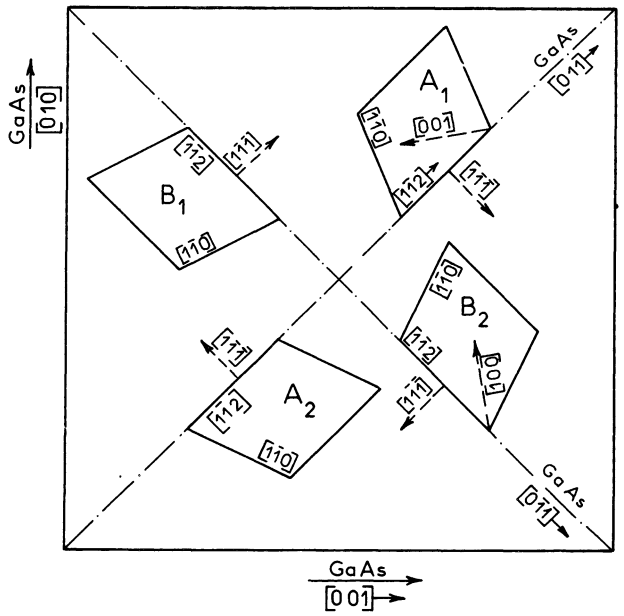

Fig. 4. — Scheme of four (110) epitaxial nickel crystals on (100) GaAs.

THIN NICKEL LAYER ON A (111) GaAs FACE. — Experiments were carried out on both (111) and $(\bar{1}\bar{1}\bar{1})$ faces of a n-GaAs single crystal in order to verify if the atomic composition of surface planes has an effect on the nickel deposition process. The experimental conditions were similar to the ones previously used for deposition on the (100) GaAs face. In fact we never detected any significant structural differences between Ni layers deposited on (111) or $(\bar{1}\bar{1}\bar{1})$ GaAs faces, however the current intensity was sligthly larger on the (111) face, indicating that the nucleation rate would be faster for Ga-rich (111) planes. Figures 6a and 6c show the RHEED diagrams of Ni deposits observed respectively under the $[11\bar{2}]$ and $[01\bar{1}]$ azimuthal directions of the (111) GaAs single crystal face. Whatever the observation azimuth, a (331) Ni reflection is always found on the sym-

Fig. 5. — HRTEM image showing the nickel (111) lattice planes on both sides of a twin (T).

metry axis of the pattern. So, the following epitaxial relation can be expressed as:

$$(331)\ \text{Ni} \ /\!/ \ (111)\ \text{GaAs} \tag{3}$$

Figures 6b and 6d are the pattern models deduced from the analysis of figures 6a and 6c. There are three equivalent positions corresponding to the three $[11\bar{2}]$ equivalent axis on the (111) GaAs surface.

In figure 6b, the pattern results from the superposition of two $[1\bar{1}0]$ Ni diagrams which are symmetrically positioned versus the [111] GaAs axis with a common $[33\bar{1}]$ diffraction spot.

The two [110] Ni axis are tilted with a angle $\theta = 13.3°$ on both sides of the symetry axis. In consequence one can describe the epitaxial relation as resulting of the contact of a $(33\bar{1})$ Ni plane with the (111) GaAs face but it is also possible to consider that nickel is limited by oblique (110) facets giving a tilt boundary containing vacancies. This boundary structure would facilitate the fitting between the two crystal networks.

THICK NICKEL DEPOSITS ON (111) GaAs FACES. — In this case too, the thick layers keep the epitaxial relation defined in the first Ni underlayer. In figure 7 one can see characteristic triangular microdomains (mean size: 20 to 30 nm) which correspond to the various equivalent epitaxial positions. In the same manner, the associated transmission diffraction pattern exhibits a sixfold symmetry due to the superposition of the equivalent Ni diagrams. Knowing that the (331) Ni reticular plane is very close to a (110) plane and thanks to the elongation of diffraction nodes in the direction of the incident beam, indexation of transmission diffraction pattern can be interpreted as the superposition of three (110) Ni diagrams and the corresponding symmetric diagrams. The second epitaxial relation can therefore be expressed by the following equation:

$$[1\bar{1}0]\ \text{Ni} \ /\!/ \ [11\bar{2}]\ \text{GaAs}$$

with the possibility to permute the indices of $[11\bar{2}]$ GaAs axis, and to consider the symmetric positions of the (110) Ni unit cell.

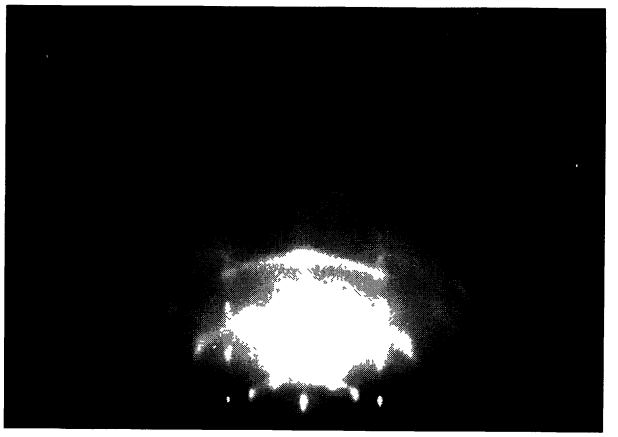

a)

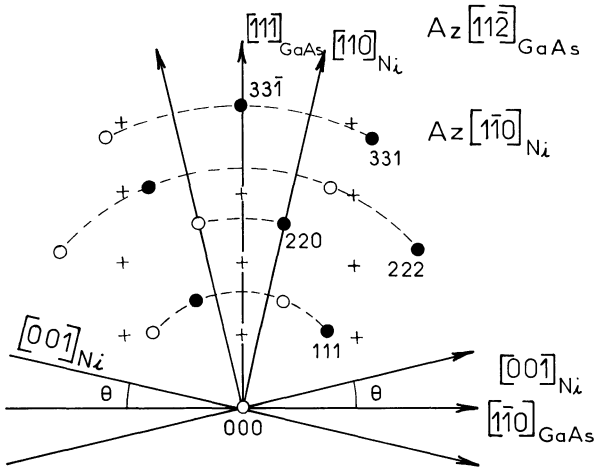

b)

Fig. 6. — RHEED diagrams obtained with a thin nickel film deposited on (111) n-GaAs. (a) Observation in the $[11\bar{2}]$ GaAs azimuth. (b) Indexation of the diagram (a). (c) Observation in the $[01\bar{1}]$ GaAs azimuth. (d) Indexation of the diagram (c). (+) GaAs diffraction spots, (o) and (•) Ni diffraction spots.

Discussion.

According to previous experimental investigations, layers of various metal such as Ru, Pt, Ag or Pb electrodeposited on GaAs single crystal are made of tiny independant crystallites which don't have any epitaxial relation with the substrate [6]. In the present study, the formation of continuous epitaxial nickel films is certainly due to the strong reactivity between nickel and gallium arsenide. This phenomenon was also observed with nickel layers prepared by condensation in ultra high vacuum conditions on a heated GaAs substrate. A ternary compound of few atomic layers was found and identified as Ni_2GaAs by Ogawa [7] and as Ni_3GaAs by Sands et al. [8]. In the case of nickel electrodeposition, Weil [9] and Thundat [10] assumed also a strong interaction with the substrate resulting in the formation of a 2D layer. In the present case we can assume that the

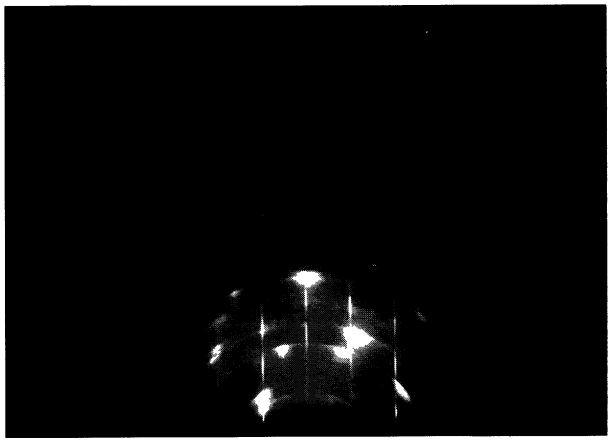

c)

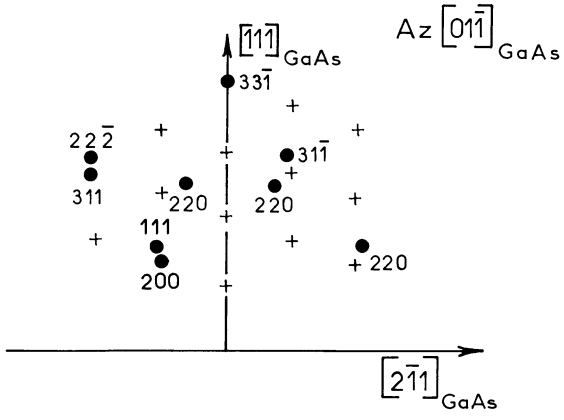

d)

Fig. 6. — continued.

incorporation of a freshly reduced nickel atom is much more easy on the border of the first 2D nuclei, at the contact with the GaAs substrate, than on the top of the nuclei. In these conditions a fast lateral growth is induced until the complete coverage of the electrode surface. The thickness of this underlayer is determined by the ratio between the probability p_b to incorporate a new atom at the border and the probability p_n to form a new 2D nucleus over the first monoatomic islands. It is well known that nickel growth tends to be inhibited by various chemical species such as atomic or molecular hydrogen and also by reaction intermediates such as $NiOH^+$ which are strongly adsorbed on the Ni surface [11]. We can assume that this adsorption tends to hinder drastically p_n and therefore we may understand why the current is strongly reduced when the electrode surface is entirely covered by the first layer. In the next step, a 3D nucleation appears necessary to overcome underlayer surface inhibition. The crystal growth is now possible owing to the continuous presence of incorporations sites such as kinks or emergences of crystals defects (dislocations, twin boundaries) [12] at the surface of 3D crystallites. We gave evidence that 3D nuclei have the same crystal orientation that the first nickel underlayer. On (100) GaAs face, (110)

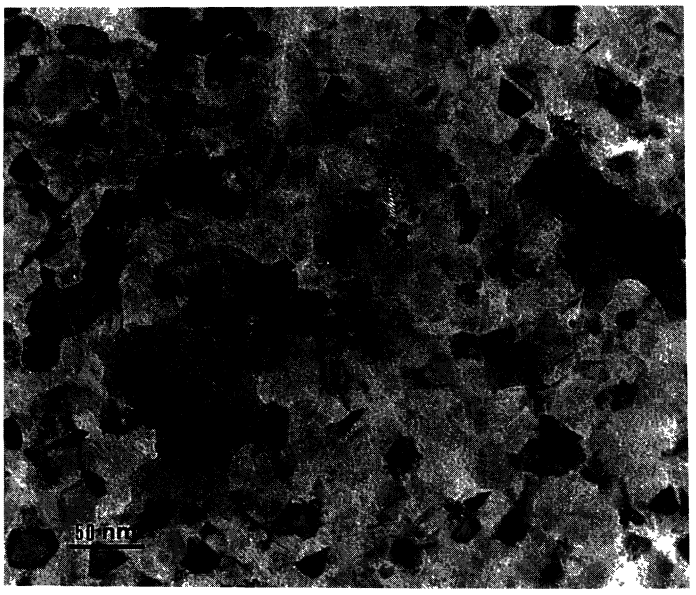

a)

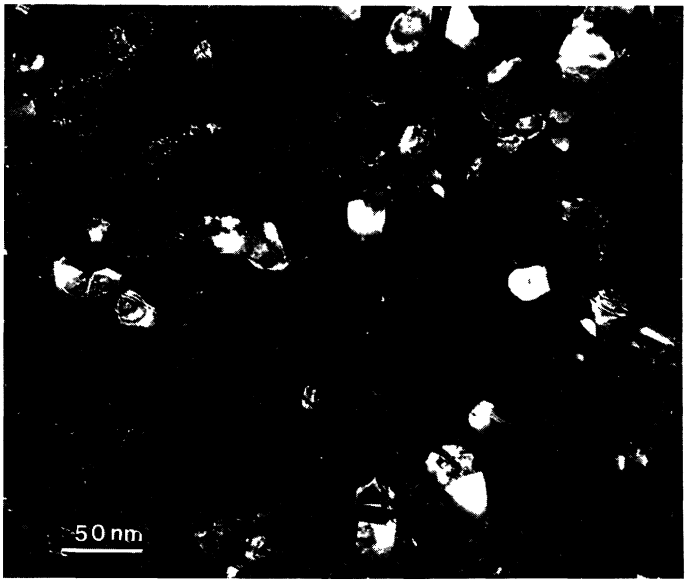

b)

Fig. 7. — TEM observation of a thick nickel deposit on (111) n-GaAs; $V_d = -0.9$ V/SCE, $t_d = 15$ s. (a) Bright field image. (b) Dark field image. (c) Microdiffraction diagram corresponding to (a). (d) Indexation of diagram (c); (o) GaAs (220) dots, (•) Ni diffraction spots in epitaxial position, (+) other Ni diffraction spots.

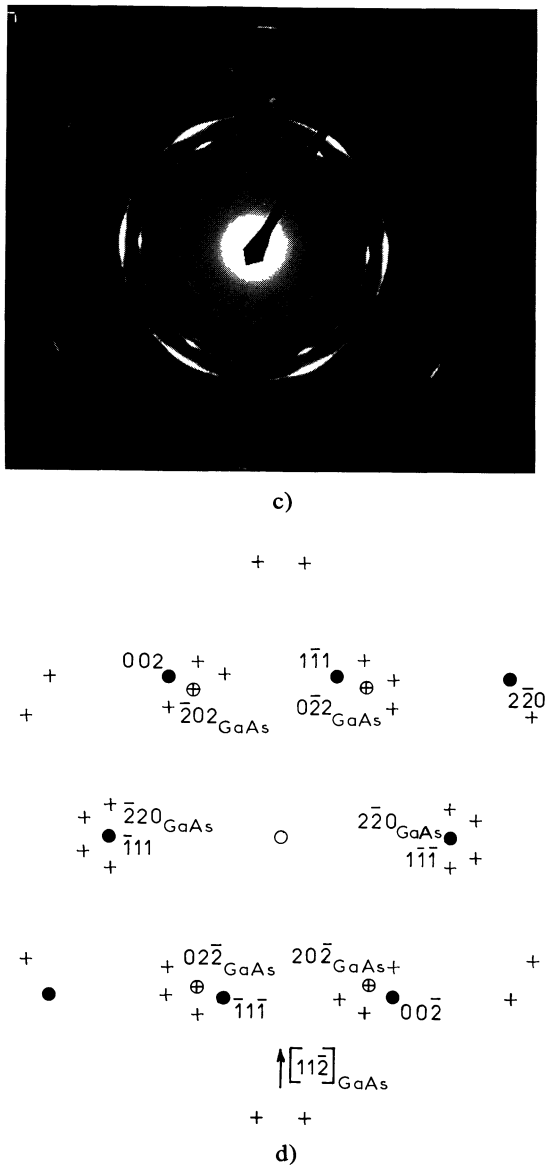

Fig. 7. — continued.

Ni planes are parallel to the substrate according to equations (1) and (2). On the (111) GaAs face it appears that the relatively dense (110) Ni planes are not exactly parallel to the substrate, as it was observed for nickel deposited by evaporation in UHV onto a (111) Silicon single crystal [13], but they are obliquely positioned in such a way that a vicinal (331) plane is parallel to the substrate. This structure is certainly less strong than the (110) Ni//(100) GaAs epitaxy, on account of the vacancy character of the boundary.

Conclusion.

Owing to TEM and RHEED observations carried out in conjunction with analysis of current transients resulting from potentiostatic pulses, it was proved that nickel layer electrochemically deposited on a GaAs single crystal face, are formed in a two step epitaxial process. During the first step, a 2D nucleation followed by a lateral growth gives a 2-4 monolayers epitaxial Ni film. When the surface is completly covered by this first underlayer, a 3D nucleation occurs and keeps the same epitaxial orientation. In every cases, after the coalescence of crystallites, a mosaic structure with numerous twin boundaries is obtained due to the presence of several equivalent positioning of 2D and 3D nuclei with respect to GaAs substrate.

References

[1] ALLONGUE P., SOUTEYRAND E., *J. Electroanal. Chem.* **286** (1990) 217.
[2] GUNAAWARDENA G., HILLS G., MONTENEGRO I., *J. Electroanal. Chem.* **138** (1982) 225.
[3] TREVISAN-SOUTEYRAND E., MAURIN G., MERCIER D., *J. Electroanal. Chem.* **161** (1984) 17.
[4] HARRISON J.A., J. Electroanal. Chem., **18** (1968) 337.
[5] Epitaxial growth, Materials Science Series, J.W. Matthews Ed. (Academic Press, New York, 1975).
[6] ALLONGUE P., SOUTEYRAND E., ALLEMAND L., *J. Electrochem. Soc.* **136** (1989) 1027.
[7] OGAWA M., *Thin Solid Films* **70** (1980) 181.
[8] SANDS T., KERAMIDAS V.G., YU A.J., GRONSKY R., WASHBURN J., *J. Mater. Res.* **2** (1987) 262.
[9] WEIL R., STANKO G.J., MOSER D.E., *Plating Surf. Finishing* **63** (1976) 34.
[10] THUNDAT T., NAGAHARA L.A., LINDSAY S.M., *J. Vac. Sci. Technolog. A* **8** (1190) 539.
[11] WIART R., *Oberfläche Surf.* **9** (1968) 275.
[12] FROMENT M., MAURIN G., *J. Microsc. Spectrosc. Electron.* **12** (1987) 379.
[13] WRAY L., PRUTTON M., *Thin Solid Films* **15** (1973) 173.